Nb-Doped MXene With Enhanced Energy Storage Capacity and Stability

Mahjabeen Fatima[1], Jameela Fatheema[1], Nasbah B. Monir[1], Ahmad Hassan Siddique[2], Bushra Khan[1], Amjad Islam[3], Deji Akinwande[4] and Syed Rizwan[1]*

[1] Physics Characterization and Simulations Lab (PCSL), School of Natural Sciences (SNS), National University of Sciences & Technology (NUST), Islamabad, Pakistan, [2] Key Laboratory of Graphene Technologies and Applications of Zhejiang Province, Ningbo Institute of Materials Technology and Engineering (NIMTE), Ningbo, China, [3] College of Materials Engineering, Fujian Agriculture and Forestry University, Fuzhou, China, [4] Microelectronics Research Center, The University of Texas at Austin, Austin, TX, United States

MXenes present unique features as materials for energy storage; however, limited interlayer distance, and structural stability with ongoing cycling limit their applications. Here, we have developed a unique method involving incorporating Nb atoms into MXene (Ti_3C_2) to enhance its ability to achieve higher ionic storage and longer stability. Computational analysis using density functional theory was performed that explained the material structure, electronic structure, band structure, and density of states in atomistic detail. Nb-doped MXene showed a good charge storage capacity of 442.7 F/g, which makes it applicable in a supercapacitor. X-ray diffraction (XRD) indicated c-lattice parameter enhancement after Nb-doping in MXene (from $19.2A°$ to $23.4A°$), which showed the effect of the introduction of an element with a larger ionic radius (Nb). Also, the bandgap changes from 0.9 eV for pristine MXene to 0.1 eV for Nb-doped MXene, which indicates that the latter has the signature of increased conductivity due to more metallic nature, in support of the experimental results. This work presents not only the effect of doping in MXene but also helps to explain the phenomena involved in changes in physical parameters, advancing the field of energy storage based on 2D materials.

Keywords: MXene, Nb doped MXene, 2D titanium carbide, supercapacitors, density functional theory

INTRODUCTION

In the last decade, chemical processes have been developed to successfully produce a versatile family of two-dimensional (2D) transition metal carbides, nitrides, and carbonitrides, termed MXenes, from their parent layered MAX phases (Lei et al., 2015). Additionally, some unique and favorable properties of MXene have been discovered, creating tremendous opportunities for research and development, with potential applications in various fields such as energy storage devices, magnetic sensors, optoelectronic devices, etc. (Novoselov et al., 2004; Mariano et al., 2016; Zhuang et al., 2018; Sunaina et al., 2019). To date, more than 70 MAX phases have been reported, but the most popular and well-established of them include Ti_3AlC_2, Ti_2AlC, $(Ti_{0.5}, Nb_{0.5})_2C$, $(V_{0.5}, Cr_{0.5})_3C_2$, Ti_3CN, Ta_4AlC_3, Nb_2AlC, V_2AlC, and Nb_4AlC_3 (Geim and Novoselov, 2007; Guo and Dong, 2011; Naguib et al., 2011a, 2012, 2013; Singh et al., 2011; Kuila et al., 2012; Tang and Zhou, 2013; Jing et al., 2014; Naguib and Gogotsi, 2015). The MAX titanium aluminum carbide is a layered, hexagonal carbide, or nitride form of compound, having the general formula "$M_{n+1}AX_n$",

where $n = 1, 2, 3$ and where M is a transition metal, A is an A-group element, and X represents carbon or nitrogen or a combination of both (Shein and Ivanovskii, 2013). Titanium aluminum carbide is used to make a daughter compound, i.e., MXene (Ti$_3$C$_2$), by eliminating aluminum from the layers of MAX to create paths for conduction of electrons along two dimensions. Notably, the outer surfaces of the exfoliated layers of MXene are always terminated by F, OH, and/or O groups during the chemical etching process (Hu et al., 2014). Henceforth, the terminated MXene species will be referred to as M$_{n+1}$X$_n$T$_x$, where T represents the surface groups (F, OH, and/or O) and "x" is the number of terminations (Naguib et al., 2011b).

MXene, having higher conductivity compared to graphene, is advantageous for usage in the charging/discharging process in batteries (Nowak and Ziolek, 1999). MXene is preferred over graphene because of its better and modified properties, such as high specific surface area, electronic structure, and properties that differ from the bulk counterparts due to low dimensionality, i.e., a 2D lamellar structure, but also due to possessing hydrophilic surface properties and good electrical conductivity (Tang et al., 2018). Hence, MXene can be considered the best known 2D material for energy storage purposes.

Doping is performed to introduce impurities into 2D materials in order to induce desirable properties in the target material. After doping, many effects, such as an increase in the c-lattice parameter (c-LP) and the introduction of defects and impurities, can be obtained, which is useful for energy storage applications. Niobium (Nb) belongs to the fifth group of transition metals, with the oxidation state of +5 and a partially filled d-orbital. The incomplete d-orbital contributes to the stronger metal–metal bonding in the bulk material. It has a comparable ionic size to that of titanium (Ti; the ionic size of Nb has been reported to be 0.098 nm, while that of Ti is 0.097 nm), which makes it a suitable candidate to dope into Ti$_3$C$_2$ MXene (Tariq et al., 2018; Dashuai et al., 2019). Nb is highly reactive, which is useful in helping it attached to the surface of MXene. This article reports on an experimental and computational study of the effect of Nb-doping of Ti$_3$C$_2$ MXene from structural and morphological perspectives and for energy storage applications, such as in supercapacitors and lithium-ion batteries. This study helps reveal the possibility of increasing electronic conductivity in batteries by using doped MXene.

The main objective was to study the trend of MXene when doped with a transition metal, i.e., Nb, in order to observe the effects on the bandgap, as for pristine MXene, the bandgap was calculated to be 1.2 eV, which changed to 0.1 eV when doped with Nb.

EXPERIMENT AND METHODS

MXene was formed from the aluminum etching of MAX Compound (Ti$_3$AlC$_2$). First, 10 g of MAX was dissolved in 230 ml of Hydrofluoric acid (HF, 39% wt%) in a Teflon beaker under constant magnetic stirring of 66 h at room temperature. After that time period, washing of MXene was performed by deionized water and ethanol several times to lower the pH of the obtained

product. Washing was carried out in order to remove the acidic residues from MXene, and thus, after obtaining a pH of 6, vacuum filtration was performed to obtain the final product in the form of 2D layered MXene (Ti$_3$C$_2$), which was then dried in a vacuum oven for 16 h at 55°C.

For the preparation of Nb-doped MXene, etched MXene, i.e., Ti$_3$C$_2$, was treated with KMnO$_4$ and ethylene glycol in order to secure MXene sheets from distortion. Then, 100 ml of Nb$_2$O$_5$ was prepared in 50 ml deionized water by introducing 25 ml ethyl glycol and 25 ml acetic acid into the deionized water at a ratio of 1:1; 200 ml Ti$_3$C$_2$ powder was then dispersed in the 100 ml aqueous solution of Nb$_2$O$_5$ under magnetic stirring at room temperature for 6 h. Next, 100 ml of KMnO$_4$ aqueous solution was slowly added to the above solution and stirred for 30 min. After the addition of KMnO$_4$, the color of the solution changed from grayish to dark purple, and, by the end, it turned dark gray. The solution was then rinsed with ethanol and deionized water three times, and extraction of precipitate was performed by vacuum filtration. It was then dried in a vacuum at 80°C for 24 h to obtain the powdered form of the desired material.

For the X-Ray Diffraction (XRD) study of the samples, a Bruker D8 Advance system was used to observe and analyze the diffraction peaks as well as the crystallinity. Additionally, for the study of morphology and elemental analysis, energy dispersive spectroscopy (EDS) was performed with a TESCAN VEGA 3. Transmission electron microscopy (with a ThermoFisher Talos F200X at an operation voltage of 200 keV) was used for analysis of the Nb-doped MXene to obtain high-resolution images. Cyclic voltammeter measurements were carried out using a Gamry Interface 1000E potentiostat, using Ag/AgCl as the electrodes. Moreover, the theoretical study is based on density functional theory. For simulations, the WIEN2k package was used, which employs the Full Potential Linear Augmented Plane Wave method (FP-LAPW) (Wimmer et al., 1981; Blaha et al., 2001). Firstly, the structure of Ti$_3$C$_2$ was generated and optimized at 500 k-points (k-mesh 14 × 14 × 2) using the Generalized Gradient Approximation PBE as well as WC GGA (Perdew et al., 1996; Wu and Cohen, 2016). The ground state of the structure was achieved by fully relaxing the internal coordinates. Subsequently, the band structure, density of states, and electron density were calculated using the GGA-PBE of the relaxed structure. To better understand the experimental results and structure, the c-parameter was increased up to 19.2 Å, and the band structure, density of states, and electron density were calculated. The next step was to simulate and optimize the Nb-doped MXene, for which WC-GGA was used at 500 k-points. The electron density, density of states, and band structure were studied for both the ground state structure and the structure based on the experimental parameters, i.e., c = 23.4 Å using the GGA-PBE functional.

RESULTS AND DISCUSSION

Structural analysis of the Nb-doped sample was performed by X-ray diffractometer. The XRD graphs of MXene and Nb-doped MXene are shown in **Figure 1A**. It can be seen that the
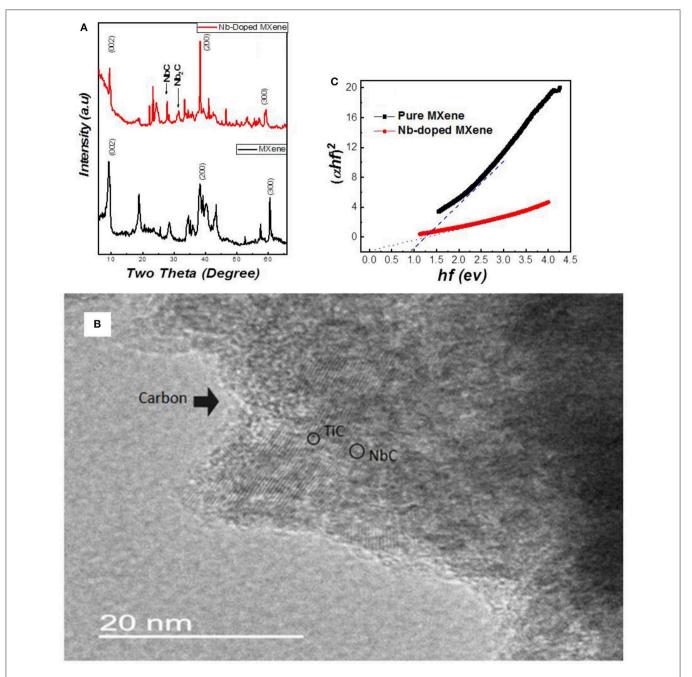
FIGURE 1 | (A) X-ray diffraction of undoped (black) and Nb-doped (red) Ti$_3$C$_2$ MXene. **(B)** Transmission electron microscopy image of Nb-doped MXene. **(C)** Comparison of the bandgaps for undoped (black) and Nb-doped (red) Ti$_3$C$_2$ MXene.

well-reported peaks of Ti$_3$C$_2$-MXene at 9, 18.8^0, and 60.4^0 are suppressed, with the appearance of new broader peaks. Due to the substitutional doping of Nb, two peaks appear at 28.5^0 and 35.1^0, which are referred to as niobium carbide (NbC, Nb$_2$C) in the literature (Ivanovskii, 2007; Qing et al., 2012; Li et al., 2015, 2018; Su et al., 2018).

The peak appearing at 9.5^0 in MXene is shifted to a lower angle, 9.3^0. At 60^0, there is a peak that is sharp and intense in the MXene but has decreased intensity in Nb-doped MXene, which

is the result of the doping. In **Figure 1B**, carbon gives rough edges in the structure while the two contrasts i.e., light and dark pattern represents NbC and TiC respectively. Moreover Niobium replacing Titanium in MXene sheets gives Nb2CTx thin layers (Jia et al., 2011; Zhang et al., 2016). The presence of Nb in MXene has decreased the intensity of the MXene peak, which indicates that the amount of lattice defects has been increased (Tarascon and Armand, 2001). The peaks were analyzed analytically, and a comparison was made between the lattice parameters for

undoped and doped samples. This shows that a-LP is 5.33A°
for Ti$_3$C$_2$Tx and 5.28A° for Nb-Ti$_3$C$_2$, which is due to a slight
ionic radii mismatch (the ionic radii of Nb and Ti are 0.069 nm
and 0.068 nm, respectively). The value calculated for c-LP for
Ti$_3$C$_2$ is 19.2A°, and that for Nb-Ti$_3$C$_2$ is 23.4A°, which shows
intercalation between the MXene sheets.

Figure 1C represents the bandgaps of the samples as
measured using UV-Vis spectroscopy through the absorbance
and transmittance values of Nb-doped MXene. Like the MXene,
Nb-doped MXene also shows a direct bandgap, as reported
previously (Zifeng et al., 2016). The graphs obtained for Nb-
doped MXene and MXene show that the bandgap has decreased
from 0.9 eV to almost 0.1 eV for Nb-doped MXene. From EDX,
it can be observed that substitutional doping of Nb occurred in
Ti$_3$C$_2$ MXene (Figure S1). After doping, the Ti peaks become
shorter with the increase in Nb peaks. Hence, we can confirm that
Nb was successfully doped into the material both as a substitution
of Ti and by penetration among the MXene sheets.

For the ground-state properties, we relaxed the structure of
Ti$_3$C$_2$ and NbTi$_2$C$_2$ by employing different exchange-correlation
functionals in WIEN2k, as shown in Figures 2a,b. In Ti$_3$C$_2$, there
are two non-equivalent Ti atoms, Ti1 and Ti2, where Ti1 occupies
(1/3,2/3,u), (2/3,1/3,v) and Ti2 is present at (0,0,0) with space
group P63/mmc. For the doped structure, Nb replaces Ti1 at one
of its Wyckoff positions.

The c-lattice parameters for relaxed structures of Ti$_3$C$_2$ and
NbTi$_2$C$_2$ were found to be 15.0334 and 15.2018 Å, respectively,
from the GGA-WC functional. The experimental and theoretical
lattice parameters for Ti$_3$C$_2$ are different by almost 4 Å, whereas,
for NbTi$_2$C$_2$, the difference is 8 Å. A similar situation is also
reported by Naguib et al. who state that the reason for this is the
instability of MXene surfaces in air, which causes bond formation
of exposed Ti with oxygen (Naguib et al., 2011a). Furthermore,
the reason for the huge difference in NbTi$_2$C$_2$ could be further
reactions in MXene, i.e., while Nb enters between the sheets, it
increases the c-parameter even more. The structures based on the
experimental parameter are shown in Figures 2c,d.

The electronic properties of these structures were also studied
computationally. Figures 2e,f shows the electron density of the
relaxed Ti$_3$C$_2$ and NbTi$_2$C$_2$. The presence of the Nb atom
changes the electron density and strengthens the bond, as Nb has
a completely filled 3d shell and a partially filled 4d shell, while Ti
only has three electrons in the 3d shell. In Figures 2g,h, when
the lattice parameter is increased, we can see that the density
becomes slightly different compared to the relaxed structures, as
layers are now farther apart than before, and the area with the
lowest electron density increases in size.

The band structure for pure MXene (Figure S2) shows
a metallic behavior, since the bandgap is represented to
be zero, whereas, from the UV-Visible Spectroscopy, we
observed a bandgap of 0.9 eV. The reason for this mismatch
in bandgap is the presence of termination groups on the
surface. After doping with Nb, we observe that, around the
Fermi level, there is an increase in the density of electrons.
Also, the bandgap for the Nb-doped structure (Figure S2)
remains zero, which is slightly more comparable to the
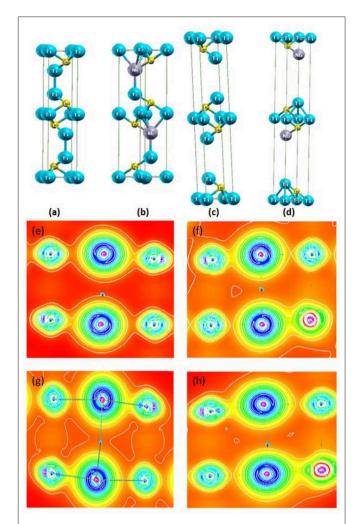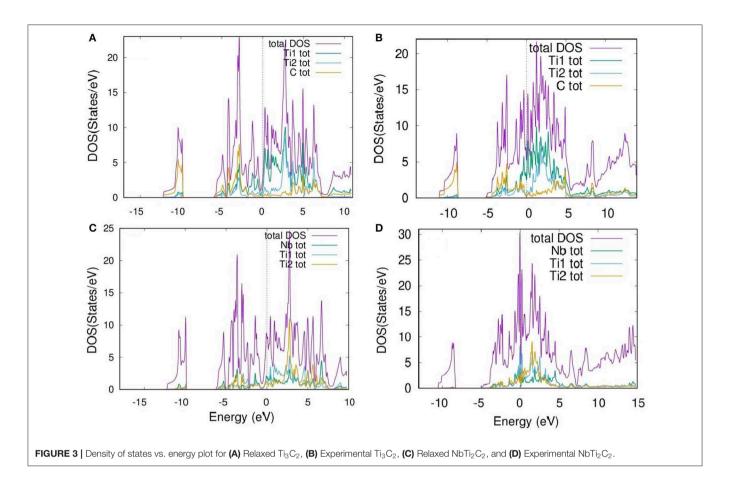experimental results.

FIGURE 2 | Structures of (a) Ti$_3$C$_2$, and (b) NbTi$_2$C$_2$ based on the relaxed
parameter and structure of (c) Ti$_3$C$_2$, and (d) NbTi$_2$C$_2$ based on the
experimental lattice parameter. Electron density of the relaxed structures for (e)
Ti$_3$C$_2$, and (f) NbTi$_2$C$_2$. Electron density of the experimental structures for (g)
Ti$_3$C$_2$, and (h) NbTi$_2$C$_2$.

For the structures with an enlarged c-parameter, we observe a
slight difference in the band structure inside the valence band.
For the purpose of pure MXene with relaxed parameters, a
pink and violet band appears at −5.5 eV, and then, for enlarged
parameters, it is shifted to −4.5eV (Figures S2A, S3A). In
contrast, for the Nb-doped structure, this shift is from −6 to
−4 eV (Figures S2B, S3B). Another point of difference is that the
density of levels around Fermi levels is greater in the Nb-doped
MXene than in the pure MXene. This is due to the electronic
configuration of Nb, which has 10 electrons in the 3d orbital
and then some more contribution from the electrons in the
4d orbital.

A density of states (DOS) vs. energy plot is presented
in Figure 3, where Figures 3A,B are for relaxed and
experimental Ti$_3$C$_2$, and Figures 3C,D are for relaxed and
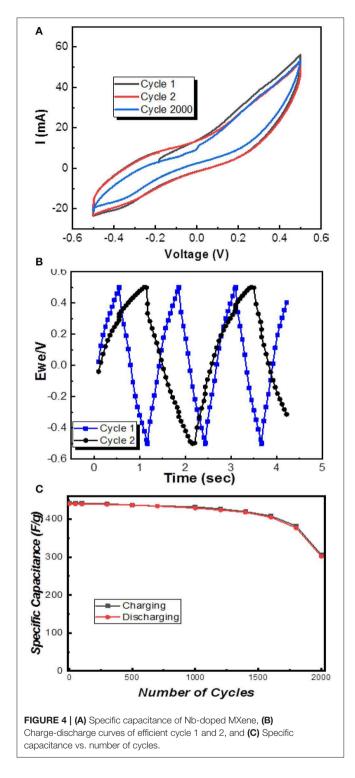experimental NbTi$_2$C$_2$. The partial DOSs for the atoms

FIGURE 3 | Density of states vs. energy plot for **(A)** Relaxed Ti$_3$C$_2$, **(B)** Experimental Ti$_3$C$_2$, **(C)** Relaxed NbTi$_2$C$_2$, and **(D)** Experimental NbTi$_2$C$_2$.

and their corresponding shells are given in **Figures S4**, **S5**. From **Figures 3A,B**, we observe that the maximum value of DOS remains almost the same. The difference comes at the point where there is shifting of a few peaks from −5 eV to the Fermi level (0 eV), and similarly for the peaks at 5 eV. **Figures S4A,B,D,E** shows that the contribution from Ti1 and Ti2 is completely due to the d-orbital as that is the only valence orbital with free electrons. The difference in the DOS for Ti1 and Ti2 of relaxed parameters and experimental parameters was determined by the shift of peaks of the d-orbital. As the c-lattice parameter increases, the hybridization or bonding of one layer with the other layer decreases, resulting in more contribution of free electrons. For carbon (**Figures S4C,D**), the s-orbital is contributing mainly at the valence band, while the p-orbital is contributing in both the valence and conduction bands, showing the hybridization of the p-orbital with the d-orbital of Ti.

Furthermore, the Nb doping increases the density of states per eV. In the relaxed structure, it increases slightly (**Figure 3C**), but as the c-parameter is increased up to 23.4 A$^\circ$, the DOS per state increases even more, especially around the Fermi energy level (**Figure 3D**). For the Nb atom, unlike the Ti atom, the contribution is not only from the d-orbital but a small amount of contribution comes also from the s-orbital, as the electronic configuration of Nb is [Kr] 4d^{4}5s^1. Besides that, for Ti1 and Ti2, the highest DOS peaks are at the Fermi energy level for given experimental parameters.

The cyclic voltammetry shows the I-V curve of Nb-doped MXene was observed at a potential window of −0.5V to +0.5V. From **Figure 4A**, the current vs. voltage graph enables the calculation of a maximum gravimetric capacitance of about 442.7 Farad/gram. This value of gravimetric capacitance of Nb-doped MXene sheets is about twice that reported for pure MXene previously (245 Farad/gram) in the literature (Li et al., 2017). The formula used was as follows:

$$C = \frac{Imax}{m(dv/dt)} \tag{1}$$

To calculate storage capacity for charge, Equation (1) was considered, which shows that Nb-doped MXene exhibits high values of specific capacitance and enhanced performance of the MXene sheets and is inclusive of other factors such as higher specific area and enhanced storage ability because of its morphology of aligned flake-like structures (Zhao et al., 2015; Xiao et al., 2016). At higher current density, K$^+$ ions, which are diffused from 6M KOH electrolyte, have abundant time to gain access and penetrate deep into the gaps available between different Nb-doped MXene layers easily, holding energetically, which leads to good a charge to discharge ratio (Chenhui et al., 2017; Ravuri et al., 2017). Also, the obtained charge-discharge triangular curves, which can be seen in **Figure 4B**, show excellent and enhanced electrode material performance with Nb-doping in

FIGURE 4 | (A) Specific capacitance of Nb-doped MXene, **(B)** Charge-discharge curves of efficient cycle 1 and 2, and **(C)** Specific capacitance vs. number of cycles.

TABLE 1 | Comparison of specific capacitance of two-dimensional materials.

Material	Charging Specific Capacitance	Electrolyte
Graphene/Polyaniline Composite (Murugan et al., 2009)	408 F/g	1M H$_2$SO$_4$
Reduced Graphene Oxide/poly 3,4-ethylenedioxythiophene (Wen et al., 2014)	213 F/g	1M H$_2$SO$_4$
MXene (Ti3C2) (Cao et al., 2017)	124 F/g	KOH
Nb-doped MXene (Ti3C2) (current work)	442.7 F/g	6M KOH

F/g, respectively, whereas that for the discharge curve for 50 cycles was recorded to be 439.8 F/g and so on, as shown in **Figure 4C**, which shows a retaining trend in the specific capacitance and capability to exhibit stable and efficient electrode performance. Note that, in **Figure 4A**, cycle 1 and 2 denote the 1st cycle and 1000th cycle, whereas cycle 2,000 denotes the 2000th cycle as shown in **Figure 4C**. This directly reveals that this material can be applied in supercapacitors because of its very high specific capacitance as compared to some other two-dimensional materials like graphene; a comparison is presented in **Table 1**. Thus, we have proposed a material that can be used for supercapacitors.

CONCLUSION

XRD analysis shows that, in addition to the peaks of MXene, we observed peaks of niobium carbide, niobium-doped MXene, and niobium-doped Ti$_3$C$_2$ MXene. Analytically, c-LP was calculated to show an increase from 19.2 to 23.4 Å. The bandgap of the prepared MXene was 0.9 eV, which decreases to 0.1 eV after being doped with Nb. Thus, the Nb-doped MXene can be considered a better conductor. In support of the experiment, computational analysis was also done that explained the electron structure, band structure, and density of states. It shows a maximum gravimetric capacitance of 442.7 Farad/gram, and the charge-discharge curves show excellent and enhanced performance for the electrode material. The present study hence suggests the unique behavior of the doped two-dimensional material bandgap, which is suitable for energy storage devices such as supercapacitors and lithium-ion batteries.

DATA AVAILABILITY STATEMENT

All datasets generated for this study are included in the article/**Supplementary Material**.

AUTHOR CONTRIBUTIONS

MF and NM prepared the samples and wrote the manuscript. JF worked on the density functional theory calculation. AS and AI helped in application characterization. BK helped

MXene. Up to 1,000 cycles, the results obtained were excellent, as the last cycle's gravimetric capacitance was 432.5 F/grams. When it was further observed up to 1,500 cycles, the results were acceptable, but in the span from 1,600 to 2,000 cycles, the specific capacitance obtained was 306.8 F/gram. The charge/discharge curve values calculated for the first cycle were 442.7 and 440.5

SUPPLEMENTARY MATERIAL

The Supplementary Material for this article can be found online at: https://www.frontiersin.org/articles/10.3389/fchem.2020.00168/full#supplementary-material

REFERENCES

Blaha, P., Schwarz, K., Madsen, G. K. H., Kvasnicka, D., and Luitz, J. (2001). *WIEN2k an Augmented Plane Wave+ Local Orbitals Program for Calculating Crystal properties.* Available online at: http://susi.theochem.tuwien.ac.at/reg_user/textbooks/usersguide.pdf

Cao, M., Wang, F., Wang, L., Wu, W., Lv, W., and Zhu, J. (2017). Room temperature oxidation of Ti3C2MXene for supercapacitor electrodes. *J. Electrochem. Soc.* 164, A3933–A3942. doi: 10.1149/2.1541714jes

Chenhui, Y., Que, W., Yin, X., Tian, Y., Yang, Y., and Que, M. (2017). Improved capacitance of nitrogen-doped delaminated two-dimensional titanium carbide by urea-assisted synthesis. *Electrochim. Acta* 225, 416–424. doi: 10.1016/j.electacta.2016.12.173

Dashuai, W., Li, F., Lian, R., Xu, J., Kan, D., Liu, Y., et al. (2019). A general atomic surface modification strategy for improving anchoring and electrocatalysis behavior of Ti3C2T2 MXene in lithium–sulfur batteries. *ACS Nano.* 13, 11078–11086. doi: 10.1021/acsnano.9b03412

Geim, A. K., and Novoselov, K. S. (2007). The rise of grapheme. *Nat. Mater.* 6, 183–191. doi: 10.1038/nmat1849

Guo, S., and Dong, S. (2011). Graphene nanosheet: synthesis, molecular engineering, thin film, hybrids, and energy and analytical applications. *Chem. Soc. Rev.* 40, 2644–2672. doi: 10.1039/c0cs00079e

Hu, J., Xu, B., Ouyang, C., Yang, S. A., and Yao, Y. (2014). Investigations on V2C and V2CX2 (X= F, OH) monolayer as a promising anode material for Li ion batteries from first-principles calculations. *J. Phys. Chem. C* 118, 24274–24281. doi: 10.1021/jp507336x

Ivanovskii, A. L. (2007). Titanium nanocarbides: synthesis and modelling. *Theor. Exp. Chem.* 43, 1–27. doi: 10.1007/s11237-007-0001-7

Jia, Z., Misra, R. D. K., O'malley, R., and Jansto, S. J. (2011). Fine-scale precipitation and mechanical properties of thin slab processed titanium–niobium bearing high strength steels. *Mater. Sci. Eng.* 528, 7077–7083. doi: 10.1016/j.msea.2011.05.073

Jing, Y., Zhou, Z., Cabrera, C. R., and Chen, Z. (2014). Graphene, inorganic graphene analogs and their composites for lithium ion batteries. *J. Mater. Chem.* 2, 12104–12122. doi: 10.1039/C4TA01033G

Kuila, T., Bose, S., Mishra, A. K., Khanra, P., Kim, N. H., and Lee, J. H. (2012). Chemical functionalization of graphene and its applications. *Pro. Mater. Sci.* 57, 1061–1105. doi: 10.1016/j.pmatsci.2012.03.002

Lei, J. C., Zhang, X., and Zhou, Z. (2015). Recent advances in MXene: preparation, properties, and applications. *Front. Phys.* 10, 276–286. doi: 10.1007/s11467-015-0493-x

Li, J., Liu, W. W., Zhou, H. M., Liu, Z. Z., Chen, B. R., and Sun, W. J. (2018). Anode material NbO for Li-ion battery and its electrochemical properties. *Rare Metals* 37, 118–122. doi: 10.1007/s12598-014-0423-z

Li, J., Yuan, X., Lin, C., Yang, Y., Xu, L., Du, X., et al. (2017). Achieving high pseudocapacitance of 2D titanium carbide (MXene) by cation intercalation and surface modification. *Adv. Energy Mater.* 7:1602725. doi: 10.1002/aenm.201602725

Li, Z., Wang, L., Sun, D., Zhang, Y., Liu, B., Hu, Q., et al. (2015). Synthesis and thermal stability of two-dimensional carbide MXene Ti3C2. *Mater. Sci. Eng.* 191, 33–40. doi: 10.1016/j.mseb.2014.10.009

Mariano, M., Mashtalir, O., Antonio, F. Q., Ryu, W. H., Deng, B., Xia, F., et al. (2016). Solution-processed titanium carbide MXene films examined as highly transparent conductors. *Nanoscale* 8, 16371–16378. doi: 10.1039/C6NR03682A

Murugan, A. V., Muraliganth, T., and Manthiram, A. (2009). Rapid, facile microwave-solvothermal synthesis of graphene nanosheets and their polyaniline nanocomposites for energy strorage. *Chem. Mater.* 21, 5004–5006. doi: 10.1021/cm902413c

Naguib, M., and Gogotsi, Y. (2015). Synthesis of two-dimensional materials by selective extraction. *Acc. Chem. Res.* 48, 128–135. doi: 10.1021/ar500346b

Naguib, M., Halim, J., Lu, J., Cook, K. M., Hultman, L., Gogotsi, Y., et al. (2013). New two-dimensional niobium and vanadium carbides as promising materials for Li-ion batteries. *J. Am. Chem. Soc.* 135, 15966–15969. doi: 10.1021/ja405735d

Naguib, M., Kurtoglu, M., Presser, V., Lu, J., Niu, J., Heon, M., et al. (2011a). Two-dimensional nanocrystals produced by exfoliation of Ti3 AlC2. *Adv. Mater.* 23 4248–4253. doi: 10.1002/adma.201102306

Naguib, M., Mashtalir, O., Carle, J., Presser, V., Lu, J., Hultman, L., et al. (2012). Two-dimensional transition metal carbides. *ACS Nano* 6, 1322–1331. doi: 10.1021/nn204153h

Naguib, M., Presser, V., Lane, N., Tallman, D., Gogotsi, Y., Lu, J., et al. (2011b). Synthesis of a new nanocrystalline titanium aluminum fluoride phase by reaction of Ti 2 AlC with hydrofluoric acid. *RSC Advances* 1, 1493–1499. doi: 10.1039/C1RA00390A

Novoselov, K. S., Geim, A. K., Morozov, S. V., Jiang, D., Zhang, Y., Dubonos, S. V., et al. (2004). Electric field effect in atomically thin carbon films. *Science* 306, 666–669. doi: 10.1126/science.1102896

Nowak, I., and Ziolek, M. (1999). Niobium compounds: preparation, characterization, and application in heterogeneous catalysis. *Chem. Rev.* 99, 3603–3624. doi: 10.1021/cr9800208

Perdew, J. P., Burke, K., and Ernzerhof, M. (1996). Generalized gradient approximation made simple. *Phys. Rev. Lett.* 77:3865. doi: 10.1103/PhysRevLett.77.3865

Qing, T., Zhou, Z., and Shen, P. (2012). Are MXenes promising anode materials for Li-ion batteries? Computational studies on electronic properties and Li storage capability of Ti3C2 and Ti3C2X2 (X= F, OH) monolayer. *J. Am. Chem. Soc.* 134, 16909–16916. doi: 10.1021/ja308463r

Ravuri, S., Kollu, P., Jeong, S. K., and Grace, A. N. (2017). Synthesis and properties of 2D-titanium carbide MXene sheets towards electrochemical energy storage applications. *Ceram. Int.* 43, 13119–13126. doi: 10.1016/j.ceramint.2017.07.003

Shein, I. R., and Ivanovskii, A. L. (2013). Graphene-like nanocarbides and nanonitrides of d metals (MXenes): synthesis, properties and simulation. *Micro Nano Lett.* 8, 59–62. doi: 10.1049/mnl.2012.0797

Singh, V., Joung, D., Zhai, L., Das, S., Khondaker, S. I., and Seal, S. (2011). Graphene based materials: past, present and future. *Pro. Mater. Sci.* 56, 1178–1271. doi: 10.1016/j.pmatsci.2011.03.003

Su, T., Peng, R., Hood, Z. D., Naguib, M., Ivanov, I. N., Keum, J. K., et al. (2018). One-step synthesis of Nb2O5/C/Nb2C (MXene) composites and their use as photocatalysts for hydrogen evolution. *Chem. Sus. Chem.* 11, 688–699. doi: 10.1002/cssc.201702317

Sunaina, R., Awan, S., Zheng, R. K., Wen, Z., Rani, M., Akinwande, D., et al. (2019). Novel room-temperature ferromagnetism in Gd-doped 2-dimensional Ti3C2Tx MXene semiconductor for spintronics. *J. Magn. Magn. Mater.* 497:165954. doi: 10.1016/j.jmmm.2019.165954

Tang, H., Hu, Q., Zheng, M., Chi, Y., Qin, X., Pang, H., et al. (2018). MXene−2D layered electrode materials for energy storage. *Pro. Nat. Sci. Mater. Int.* 28, 133–147. doi: 10.1016/j.pnsc.2018.03.003

Tang, Q., and Zhou, Z. (2013). Graphene-analogous low-dimensional materials. *Pro. Mater. Sci.* 58, 1244–1315. doi: 10.1016/j.pmatsci.2013.04.003

Tarascon, J. M., and Armand, M. (2001). Issues and challenges facing rechargeable lithium batteries. *Nature* 414:359. doi: 10.1038/35104644

Tariq, A., Ali, S. I., Akinwande, D., and Rizwan, S. (2018). Efficient visible-light photocatalysis of 2D-MXene nanohybrids with Gd3+and Sn4+codoped bismuth ferrite. *ACS Omega* 3, 13828–13836. doi: 10.1021/acsomega.8b01951

Wen, J., Jiang, Y., Yang, Y., and Li, S. (2014). Conducting polymer and reduced graphene oxide Langmuir–Blodgett films: a hybrid nanostructure for high performance electrode applications. *J. Mater. Sci: Mater. Electron.* 25, 1063–1071. doi: 10.1007/s10854-013-1687-z

Wimmer, E., Krakauer, H., Weinert, M., and Freeman, A. J. (1981). Full-potential self-consistent linearized-augmented-plane-wave method for calculating the electronic structure of molecules and surfaces: O 2 molecule. *Phys. Rev. B* 24:864. doi: 10.1103/PhysRevB.24.864

Wu, Z., and Cohen, R. E. (2016). More accurate generalized gradient approximation for solids. *Phys. Rev. B* 73:235116. doi: 10.1103/PhysRevB.73.235116

Xiao, Y., Hwang, J. Y., and Sun, Y. K. (2016). Transition metal carbide-based materials: synthesis and applications in electrochemical energy storage. *J. Mater. Chem. A* 4, 10379–10393. doi: 10.1039/C6TA03832H

Zhang, C., Beidaghi, M., Naguib, M., Lukatskaya, M. R., Zhao, M. Q., Dyatkin, B., et al. (2016). Synthesis and charge storage properties of hierarchical niobium pentoxide/carbon/niobium carbide (MXene) hybrid materials. *Chem. Mater.* 28, 3937–3943. doi: 10.1021/acs.chemmater.6b01244

Zhao, S., Kang, W., and Xue, J. (2015). MXene nanoribbons. *J. Mater. Chem. C* 3, 879–888. doi: 10.1039/C4TC01721H

Zhuang, L., Zhao, M., Lin, H., Dai, C., Ren, C., Zhang, S., et al. (2018). 2D magnetic titanium carbide MXene for cancer theranostics. *J. Mater. Chem. B* 6, 3541–3548. doi: 10.1039/C8TB00754C

Zifeng, L., Rozier, P., Duployer, B., Taberna, P. L., Anasori, B., Gogotsi, Y., et al. (2016). Electrochemical and *in-situ* X-ray diffraction studies of Ti3C2Tx MXene in ionic liquid electrolyte. *Electrochem. Commun.* 72, 50–53. doi: 10.1016/j.elecom.2016.08.023